Reaction-Induced Strain in Rigid-Rod Polymeric Fibers

Shawn Jenkins,[†] Karl I. Jacob,[†] Malcolm B. Polk,[†] Satish Kumar,*[,†] T. D. Dang,[‡] and F. E. Arnold[‡]

School of Textile and Fiber Engineering, Georgia Institute of Technology, Atlanta, Georgia 30332-0295, and AFRL, Wright Patterson Air Force Base, Dayton, Ohio 45433

Received May 3, 2000

ABSTRACT: The thermomechanical behavior of several rigid-rod polymeric fibers has been investigated. Up to 300 °C, all fibers exhibited the expected axial shrinkage on heating (CTE $\approx -6 \times 10^{-6}$ °C^{-1}). However, a pronounced increase in thermal contraction was observed at temperatures where polymer degradation or cleaving of the pendant group occurred. A degradation mechanism has been proposed that accounts for the evolved gases in PBZT and MePBZT. The accelerated shrinkage in these rigid-rod polymers is a result of decrease in the *c*-axis lattice parameter as measured via WAXD. The enhanced axial shrinkage and accompanying decrease in lattice parameter are attributed to chemical changes, and consequent cross-linking taking place within these systems which, in turn, serves to perturb the crystalline structure. The implications of this phenomenon of accelerated axial contraction, with regards to morphology, are discussed.

Introduction

The relatively poor performance of rigid-rod polymeric fibers, under compressive loading, has been recognized for some time.[1] Several attempts to improve the compressive strength of these highly oriented materials have been made, most of which involve improving interactions, intermolecular or otherwise, normal to the fiber axis. Suggested methods have included polymer infiltration,[2−5] promoting molecular entanglements through bulky side groups[6] or branching,[7] and introducing strongly associating groups.[8,9] Cross-linking has been considered the most promising approach, and as a result, an abundance of work has been performed in this area.[10−18] Cross-linking can result in a concomitant decrease in tensile properties.[13,16,19] Transverse surface cracks were observed in the skin of cross-linked MePBZT fiber,[19] and cross-linking was observed in the free annealed samples. The prevention of transverse cracks and lack of cross-linking in tension-annealed MePBZT alluded to some cross-link-induced strains being generated within the material. On the basis of atomistic simulation in MePBZT,[20] a significant axial stress was predicted upon direct phenyl−phenyl cross-linking. In this work, we report the study of reaction-induced strains in rigid-rod polymers and the concomitant role of morphology. The chemical structures of various polymers investigated are given in Figure 1 and Table 1.

Experimental Section

Fiber Spinning and Heat Treatment. Fibers were spun from polymer solutions containing 10−12 wt % polymer in polyphosphoric acid. The intrinsic viscosity of monomethyl pendent PBZT (MePBZT), dimethyl pendent PBZT (DiMePBZT), and monomethyl-PBI (MePBI) was 15, 18, and 11 dL/g, respectively. The polymer solutions were dry-jet wet spun using a plunger-driven, single-filament spinning system manufactured by Bradford University Limited. The solutions were preheated in the spinning cylinder for approximately 4 h at the spinning temperature, which ranged from 90 to 125 °C. A single-hole spinneret of diameter 250 μm and an air gap of approximately 15 cm were used in all cases. The fibers were coagulated in distilled water at room temperature. The spin draw ratios obtainable in the case of MePBZT ranged between 10 and 12. Slightly higher spin draw ratios (∼15) were possible for DiMePBZT. Spin draw ratios as high as 20 were possible in the spinning of MePBI. All fibers were soaked in distilled water for approximately 1 week. The fibers were then vacuum-dried at 100 °C overnight. As-spun and tension heat-treated PBZT, dihydroxy-PBZT (DiOHPBZT), and dihydroxy-PBI (DiOHPBI) fibers were received from Wright Patterson Air Force Base, Dayton, OH, and used as received.

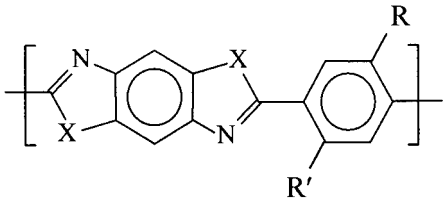

Figure 1. Generic chemical structure for the various rigid-rod polymers investigated in this work. See Table 1 for names and associated X, R, and R′ groups.

MePBZT, DiMePBZT, and MePBI fibers, spun for the present work, were tension heat-treated under a N_2 flow for 10 min at temperatures below which cross-linking is expected (i.e., ≲400 °C for MePBZT[21] and MePBI and ≲350 °C for DiMePBZT[10]). This was done to enhance crystalline order and to orient the fibers as much as possible, without inducing cross-linking. To cross-link MePBZT, fibers were free annealed at 490 °C for 20 min. Likewise, DiMePBZT fibers were free annealed at 490 °C for 10 min. For tension heat treatments, fibers were clamped on a frame and subsequently tensioned by hanging a weight on the clamp. The tensioned fibers were then heated using a tube oven with the ends plugged, to minimize air flow and heat dissipation.

Material Characterization. All thermogravimetry/mass spectrometry (TG/MS) was performed at Systems Research Laboratories, at a heating rate of 5 °C/min under 10^{-6} Torr vacuum. Ion intensity was monitored using a Finnigan quadrupole mass spectrometer. Thermal stress analysis was performed using an Instron load cell and a tube oven. Thermal stress analysis experiments were conducted on a fiber bundle (five fibers) of 3 in. length. In this way, stress could be monitored as a function of temperature. Fibers were attached to the load cell via untwisted Zylon yarn, produced by Toyobo. Zylon, that is, poly(*p*-phenylenebenzobisoxazole), is thermally stable at 525 °C in air.[22] All thermal stress analyses were

[†] Georgia Institute of Technology.
[‡] Wright Patterson Air Force Base.

10.1021/ma000780w CCC: $19.00
Published on Web 11/03/2000

Table 1. Various Rigid-Rod Polymers Studied in This Work; See Figure 1 for the Corresponding Chemical Structures

polymer system	acronym	X	R	R′
poly (*p*-phenylenebenzobisthiazole)	PBZT	S	H	H
methyl poly (*p*-phenylenebenzobisthiazole)	MePBZT	S	CH_3	H
dimethyl poly(*p*-phenylenebenzobisthiazole)	DiMePBZT	S	CH_3	CH_3
dihydroxy poly(*p*-phenylenebenzobisthiazole)	DiOHPBZT	S	OH	OH
methyl poly(*p*-phenylenebenzobisimidazole)	MePBI	NH	CH_3	H
dihydroxy poly(*p*-phenylenebenzobisimidazole)	DiOHPBI	NH	OH	OH

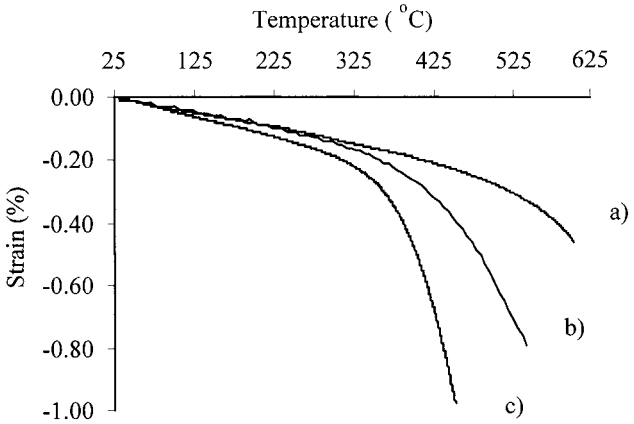

Figure 2. Shrinkage as a function of temperature for tension heat-treated (a) PBZT, (b) MePBZT, and (c) DiMePBZT fiber.

conducted in air, using a heating rate of 10 °C/min. Thermomechanical analysis was performed using a TMA from TA Instruments with the Universal data analysis software. Single fibers could be mounted and held under constant strain or load, the former being analogous to the thermal stress experiments just described. Thermomechanical analysis was performed at temperatures ranging from 25 to 650 °C in N_2.

A diffractometer mounted on Rigaku Rotaflex rotating anode generator was used to obtain all WAXD scans. $\theta/2\theta$ scans were obtained in the transmission mode using pinhole collimation. Cu Kα radiation was used in all experiments, with the X-ray generator being operated at 45 kV and 100 mA. The K_β component of the incident beam was minimized using a standard nickel filter. The smallest detector window, 1 mm × 1 mm, was used in an attempt to maximize resolution. The peak apex was used in calculating peak positions.

Results and Discussion

Thermal Analysis. From previously reported TG/MS data on MePBZT, [10] methane has been observed to be the first and primary decomposition product, evolving around 420 °C. Upon the evolution of methane, secondary processes begin to occur, which involve cleaving of main-chain bonds and lead to the evolution of H_2S, HCN, and CS_2 with increasing temperature. In the case of DiMePBZT, there is some evidence that suggests cleavage of the methyl pendent groups occurs at slightly lower temperatures (∼350 °C).[10] TG/MS analysis on DiOHPBZT and DiOHPBI shows cleavage of the hydroxy pendant groups to occur around 400 and 500 °C, respectively.[23] In both systems, H_2O, CO, and CO_2 were determined to be the initial decomposition products.

PBZT and other rigid-rod polymeric fibers are known to have negative coefficients of thermal expansion (CTE) in the range −7 to −10 ppm/°C, depending on the stress applied during testing.[24,25] Figure 2 illustrates the shrinkage of tension heat-treated PBZT, MePBZT, and DiMePBZT fiber, as a function of temperature. From this figure, the CTE of these fibers, calculated between 25 and 100 °C, can be determined to be between −5 and −7 ppm/°C. Graphite has a similarly small negative CTE in the direction of basal plane orientation, while normal to the basal plane a positive CTE has been measured.[26] This behavior has been attributed to vibrations normal to the basal plane, which cause both contraction within and expansion between the basal planes.[26] Similar motions, prior to pendent loss, may be occurring in the systems of interest here. As is evident from Figure 2, the CTE remained fairly constant up to approximately 300 °C. However, a pronounced enhancement in axial shrinkage was observed at higher temperatures, with the onset of the accelerated shrinkage occurring around 350 and 400 °C in DiMePBZT and MePBZT, respectively. These temperatures qualitatively correspond to the onset of pendant loss in the respective materials. PBZT is thermally stable to much higher temperatures, relative to MePBZT and DiMePBZT.[27] Analogously, accelerated shrinkage was not observed in PBZT until approximately 600 °C. In work done on the carbonization of PBZT fiber, pronounced shrinkage (∼7%) was observed above 700 °C and attributed to the loss of non-carbon elements.[28] However, similar to the current obserevation, the onset of shrinkage was found to begin around 600 °C. The temperature at which pronounced axial shrinkage occurs in PBZT roughly corresponds to the evolution of H_2S, the initial byproduct in thermal decomposition.[27] Further heating to 650 °C produces HCN and CS_2.

The proposed thermal degradation schemes, accounting for the evolution of H_2S, HCN, and CS_2 in PBZT, are presented in Figure 3. In the thermal decomposition of MePBZT[27] also these gases evolve in the same order, following the evolution of methane. However, the cleaving of the methyl pendant group appears to "catalyze" the degradation reaction in that the evolution of H_2S, HCN, and CS_2 in MePBZT occurs at approximately 500, 575, and 600 °C, respectively, as compared to 600 °C (H_2S) and 650 °C (HCN and CS_2) in PBZT. It is possible that hydrogen abstraction occurs more readily in MePBZT, as more hydrogen is available due to the presence of the pendant group. Moreover, with the cleaving of the pendant from the aromatic ring, more reactive species would be generated at lower temperatures, thus lowering the degradation temperature. Apparent from the proposed degradation reaction is the notion that several aromatic radicals are generated in producing H_2S. The formation of these species suggests the coupling reaction of adjacent phenyl moieties would occur in MePBZT, as reported previously.[8,21]

Figure 4a,b shows that fibers exhibit significantly reduced shrinkage after being heat-treated above the pendant cleaving temperature. This supports the hypothesis that the accelerated shrinkage is associated with the cleavage of the pendant groups and with the associated reactions that are taking place during this process. While not specifically designed to undergo reaction via labile pendent groups,[8] accelerated shrinkage is also observed in DiOHPBZT and DiOHPBI (Figure 5) at temperatures qualitatively corresponding to the onset of pendant loss for these systems. The correlation between the onset of accelerated shrinkage

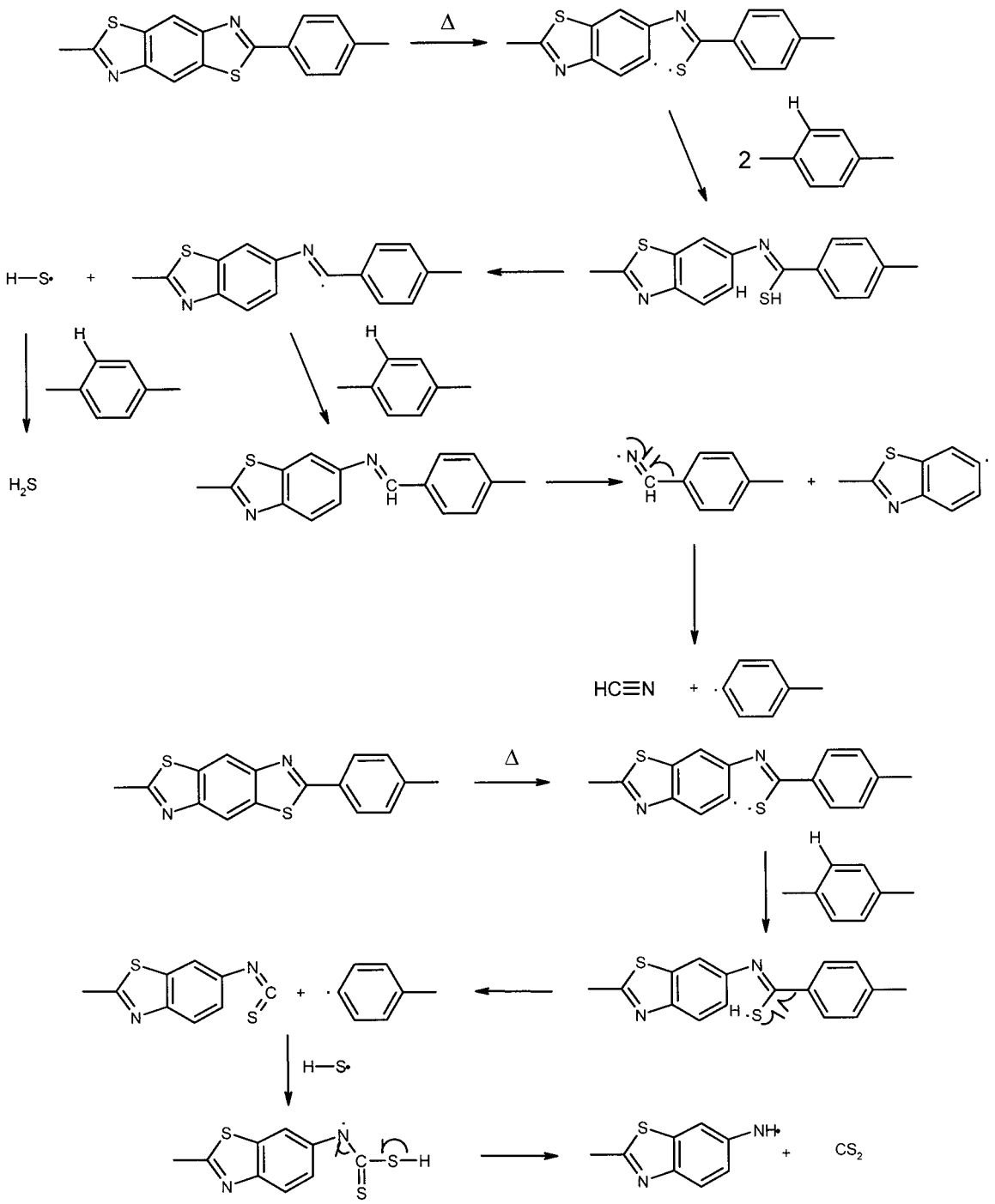

Figure 3. Thermal degradation schemes for PBZT, accounting for the evolution of H_2S, HCN, and CS_2.

and pendant cleaving or degradation temperature, for various rigid-rod polymers, is given in Figure 6.

The results of thermal stress analysis are presented in Figure 7. Stress generation was found to be linear and reversible as a function of temperature up to 525 °C in the control sample, Zylon. In MePBZT, stress was observed to increase linearly as a function of temperature up to approximately 425 °C. In contrast to Zylon, however, stress was found to increase at a greater rate as a function of temperature in MePBZT above ~400 °C. Moreover, stress was found to continue to increase despite reducing the temperature. Thus, the stress buildup in MePBZT above 425 °C is not a result of normal, reversible thermal oscillations, responsible for the negative coefficient of thermal expansion in these materials. Rather, it can be attributed to chemical changes in the material, a process that would not be reversed simply by reducing the temperature.

Isostrain and isostress experiments, the former being analogous to the thermal stress analysis just presented, were conducted on single filaments of PBZT (Figure 8) and MePBZT (Figure 9) held at a constant temperature. At 490 °C, stress relaxation is not very significant. However, at 625 °C, degradation does take place, which manifests itself in intensifying stress over time. Interestingly, stress does not increase indefinitely but rather decreases before the fiber breaks. Stress plays a minor role in the isothermal response of PBZT. At low loads, a slight contraction is notable over a relatively long period of time, possibly due to slow thermooxidative degradation. The effects of this degradation could be masked in the isostrain experiments by the compara-

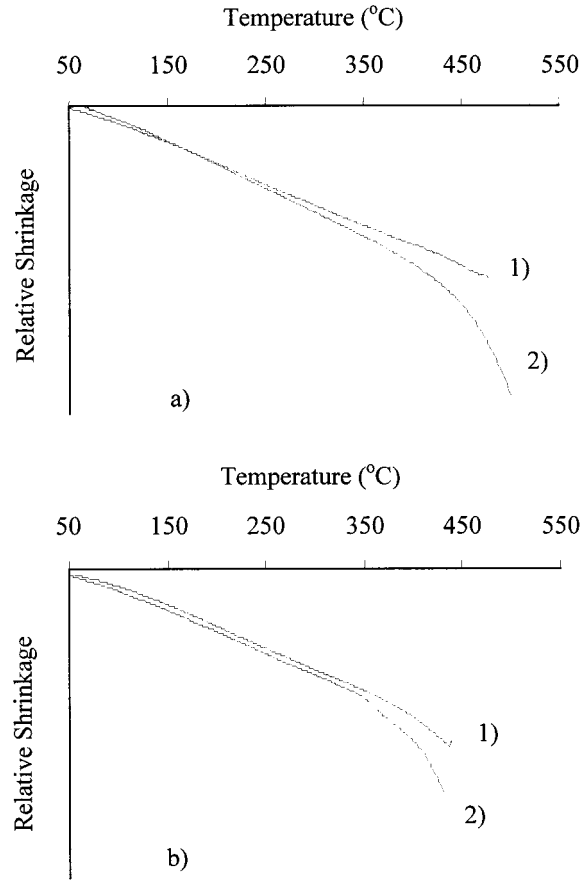

Figure 4. Relative degree of shrinkage, as measured by DMS, in (a) MePBZT and (b) DiMePBZT. In both systems, 1) and 2) refer to fibers heat-treated above (490 °C) and below (400 °C) the cross-linking temperature, respectively.

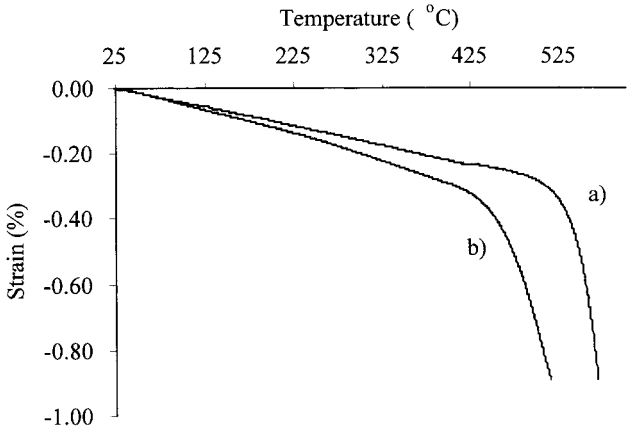

Figure 5. Shrinkage as a function of temperature for tension heat-treated (a) DiOHPBZT and DiOHPBI fibers. Fibers have been heat-treated at 400 °C.

tively high stresses imposed on the fibers. Contraction due to some slow relaxation processes cannot be ruled out, however. This contraction appears to slow as time progresses and at progressively greater loading, being either arrested or superseded by a slight expansion at 266 MPa.

In MePBZT (Figure 9a), at 0.10% strain, the stress was observed to increase initially at 490 °C and subsequently level off over time. This behavior resembles that of PBZT above the degradation temperature (Figure 8a). Qualitatively comparable results were observed in isostress measurements of both PBZT and MePBZT at 490

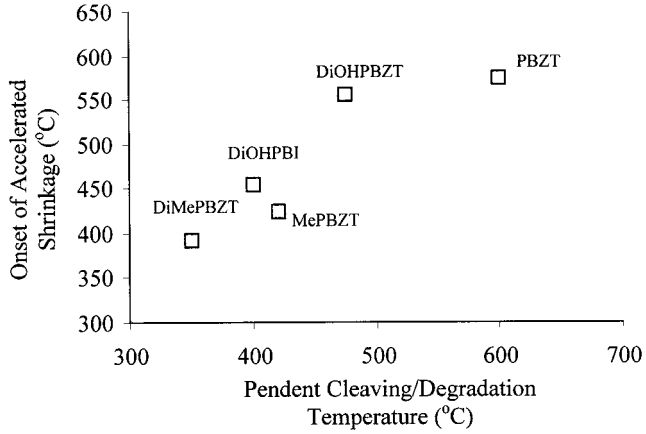

Figure 6. Onset of shrinkage as a function of pendant cleaving/degradation temperature for several pendant rigid-rod polymers. TG/MS data for MePBZT and DiMePBZT taken from ref 10. TG/MS data for DiOHPBI and DiOHPBZT obtained from ref 23. TG/MS data for PBZT taken from ref 27.

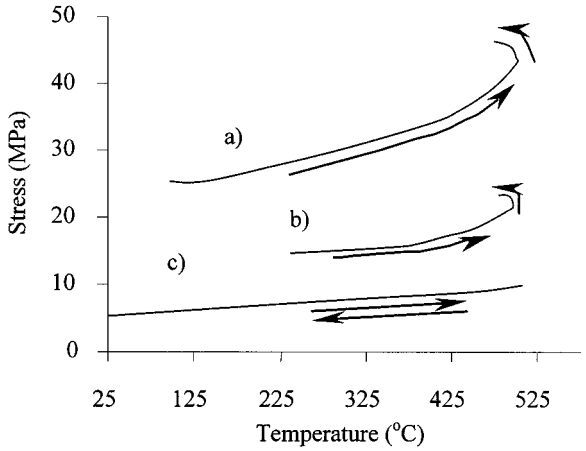

Figure 7. Thermal stress analysis on (a, b) MePBZT fiber at varying stress levels and (c) untwisted Zylon yarn (control). Note that same temperature profile is used in all three cases. Arrows indicate the direction of temperature change.

°C; however, a much more pronounced response was observed in the latter case (compare the *y*-axis scale in Figures 8b and 9b). It is evident from Figure 9 that the contraction occurring in MePBZT can be arrested almost entirely upon application of stress and even reversed at stress levels around 266 MPa. The elongation of these fibers at later times and higher stresses may be expected as a result of creep. However, any intermolecular cross-linking in MePBZT should diminish or eliminate the propensity for isothermal elongation, as slippage of one molecule past another would be restricted. However, cross-linking may be inhibited under tension,[19] and therefore elongation would be possible over time in tension heat-treated MePBZT fibers, even when subjected to cross-linking temperatures. Also notable in the isostress response of MePBZT is the continuous contraction at a low stress of 41 MPa (Figure 9b).

Wide-Angle X-ray Diffraction. Highly oriented rigid-rod polymeric fibers afford several orders of meridonal diffraction planes[29] (Figure 10). It has been suggested [30] that displacement of the specimen from the diffractometer center is often the largest single source of error in measuring peak position. For a sample displacement (δ) perpendicular to the diffraction plane normal, it has been shown[31] that

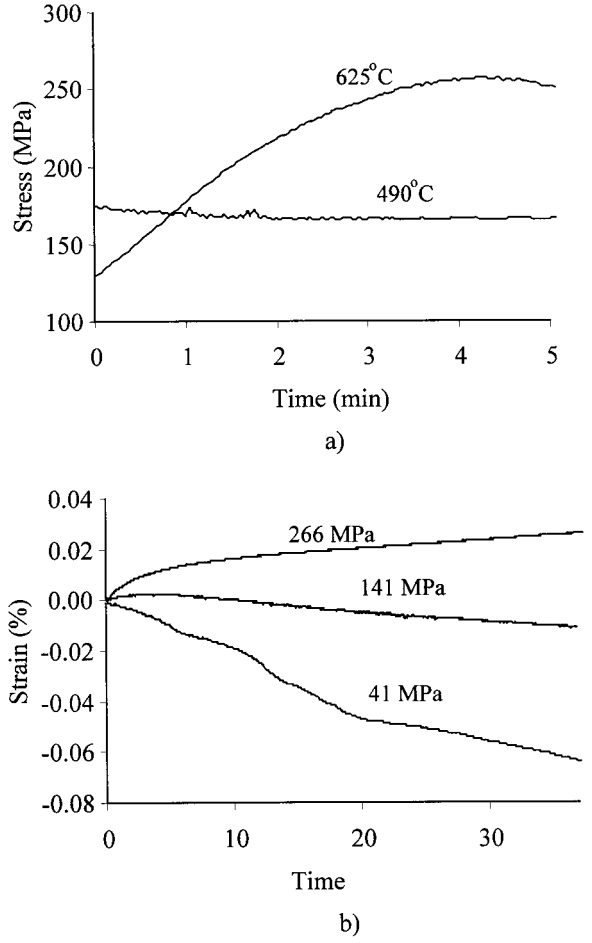

Figure 8. (a) Isostrain ($\epsilon = 0.03\%$) measurement on heat-treated PBZT fiber at two different temperatures. (b) Isostress measurements (at $T = 490$ °C) on heat-treated PBZT fiber.

$$\frac{\Delta d}{d} = -\frac{\delta}{R_0}\frac{\cos^2\theta}{\sin\theta}$$

where R_0 is the diffractometer radius and Δd is the error in measured d spacing. The utility of this equation lies in plotting a particular lattice parameter, calculated from various orders of diffraction, as a function of $\cos^2\theta/\sin\theta$. By extrapolating $\cos^2\theta/\sin\theta \rightarrow 0$, one can obtain a value for the lattice parameter which is corrected for sample displacement.

In rigid-rod polymers the analysis can be applied effectively, as multiple orders of parallel diffraction planes are available. Specifically, these diffraction planes enable direct measurement of the *c*-axis lattice parameter. If the accelerated shrinkage originates as a result of structural perturbations on the order of lattice dimensions, such perturbations would be observable from WAXD. However, if said shrinkage occurs due to the onset of some increased mobility (i.e., entropy considerations), no change in the crystalline *c*-axis lattice parameter would be expected. The notion of flexibility may be dismissed, perhaps naively, from a cursory glance of the chemical make up of these polymers. However, ribbonlike motions are thought to take place in these molecules in both solution and solid state.[32,33] These ribbonlike motions would explain the expansion perpendicular to the orientation direction observed on heating these rigid-rod polymers.[34] This is illustrated in Figure 11, where an increase in equatorial *d* spacings (i.e., arising from planes parallel to the fiber

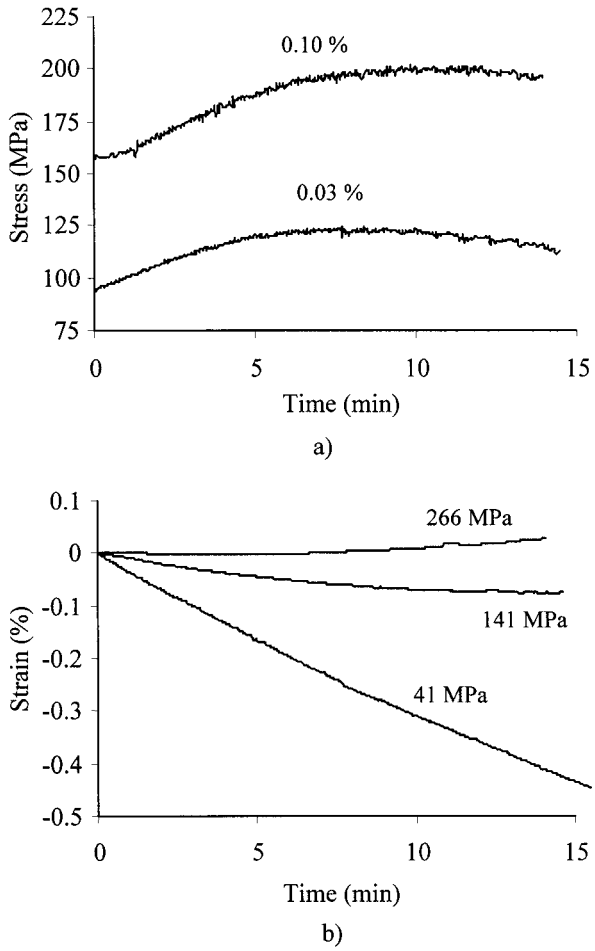

Figure 9. (a) Isostrain and (b) isostress experiments (at $T = 490$ °C) on MePBZT fiber tension heat-treated at 400 °C.

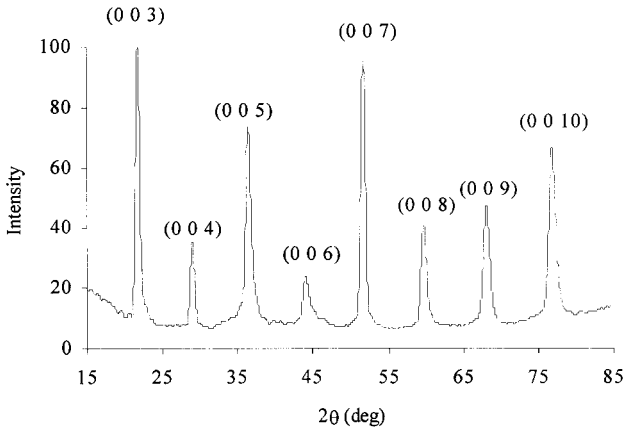

Figure 10. Meridional WAXD scan of tension heat-treated PBZT fiber with diffraction planes labeled.

axis) is observed in both the rigid-rod polymers of PBZT and PBO. Irrespective of these motions, upon cleaving a main chain bond, the polymer chain would be able to adopt new conformations energetically forbidden prior to the bond breaking. Thus, the ability to observe changes in the *c*-axis lattice parameter was of interest.

In the present work, $\theta/2\theta$ WAXD scans were obtained in transmission geometry. In addition, the displacement of the sample was not necessarily parallel to the diffraction plane normal. These two factors were thought to set the current problem of sample displacement apart from that described previously.[30] However, as reported in the Appendix, the functional form of the error in

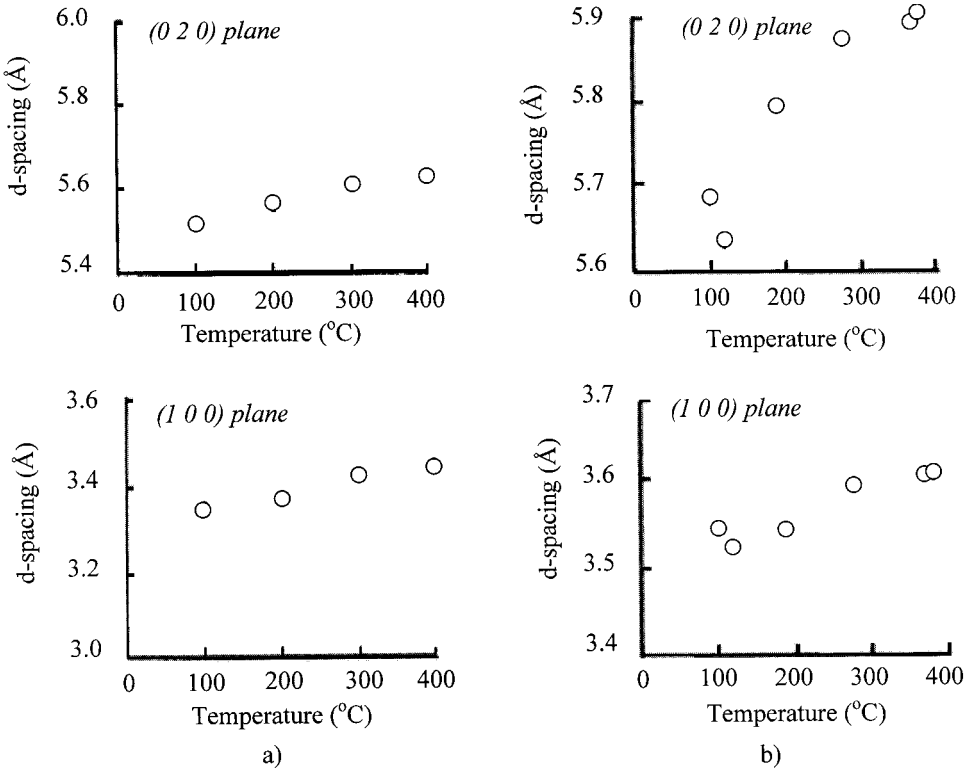

Figure 11. Variation in *d* spacings of the (1 0 0) and (0 2 0) equatorial reflections in as-spun (a) PBO and (b) PBZT fibers.

Table 2. Extrapolated Value of the *c* Lattice Parameter for Various Rigid-Rod Systems and the Corresponding R^2 Value for the Linear Least-Squares Fit; the Relevant Data Are Given in Figure 12

system	heat treatment temp (°C)	lattice parameter (Å)	R^2
PBZT	400 (tension)	12.43	0.99
	575 (free)	12.46	0.99
MePBZT	400 (tension)	12.45	0.97
	490 (free)	12.41	0.99
DiMePBZT	350 (tension)	12.48	0.95
	490 (free)	12.44	0.96
MePBI	400 (tension)	12.09	0.97
	490 (free)	11.99	0.94

measured *d* spacing as a function of θ in transmission geometry was found to be identical to that in reflection. The *c* lattice parameters, calculated for PBZT, MePBZT, and DiMePBZT, are plotted as a function of $\cos^2\theta/\sin\theta$ in Figure 12. Apparent from this figure and the R^2 values shown in Table 2, a fairly linear fit could be obtained for each data set, lending credence to the assumption that sample displacement is the largest source of error. It should be mentioned that the fit for all the PBZT-type systems neglects the (0 0 6) peak. In a majority of the analyses, this peak was observed to lie off the regression line. This was thought to be a consequence of the asymmetry in the (0 0 6) diffraction peak and associated error in using the peak apex in determining peak positions. In either case, the trends were left unchanged, and relative values were found to be only moderately influenced. In the case of MePBI and DiMePBZT, additional peaks at moderate or low 2θ values were neglected due to their low intensity or complete disappearance, which made peak position assignment difficult. Peaks at higher 2θ positions are inherently less influenced by sample displacement and were never neglected when present. In all cases, at least five orders of diffraction were used for extrapolation purposes.

Table 2 lists the extrapolated values of the lattice parameter, in addition to the R^2 values for the linear least-squares fit of each data set. Cullity[30] reports that an accuracy of 0.01 Å should be achievable with this method. In our experiments, values were found to be reproducible to this degree. The *c*-axis lattice parameter has been reported previously to be 12.514 Å in PBZT fiber tension heat-treated at temperatures as high as 700 °C.[35] In the present work, heat-treated fiber analyzed as-received from the Air Force Research Laboratory was found to have a lattice parameter value of 12.43 Å. Subsequent heat treatment without tension at 575 °C yielded a *c*-axis lattice parameter of 12.46 Å. In the case of un-cross-linked MePBZT, fibers were found to have a *c*-axis lattice parameter of 12.45 Å. Un-cross-linked DiMePBZT fiber yielded the highest value of this lattice parameter at 12.48 Å. It is believed that the difference in measured lattice parameter between each of the systems studied here, in addition to the discrepancy relative to the reported value for PBZT,[35] lies in the difference in tension heat treatment procedures. In the present work, such treatments were carried out in a batch process, allowing for nonuniformities in stress from sample to sample and potentially slight differences in heating profiles and times. In general, it was observed that PBZT fibers heated at higher temperatures for longer times resulted in slight increases in the lattice parameter. On the contrary, *c*-axis lattice parameter in MePBZT decreased by approximately 0.3% on free annealing at cross-linking temperatures. Similar results were observed in DiMePBZT, in which case the lattice parameter decreased from 12.48 to 12.44 Å. The absence of a comparable decrease in the lattice parameter of PBZT, free annealed at 575 °C, suggests that the decrease in lattice parameter in MePBZT and DiMePBZT is due to reactions occurring within the material. The *c*-axis lattice parameter for MePBI was measured to be 12.09 Å. By comparison, the *c*-axis lattice param-

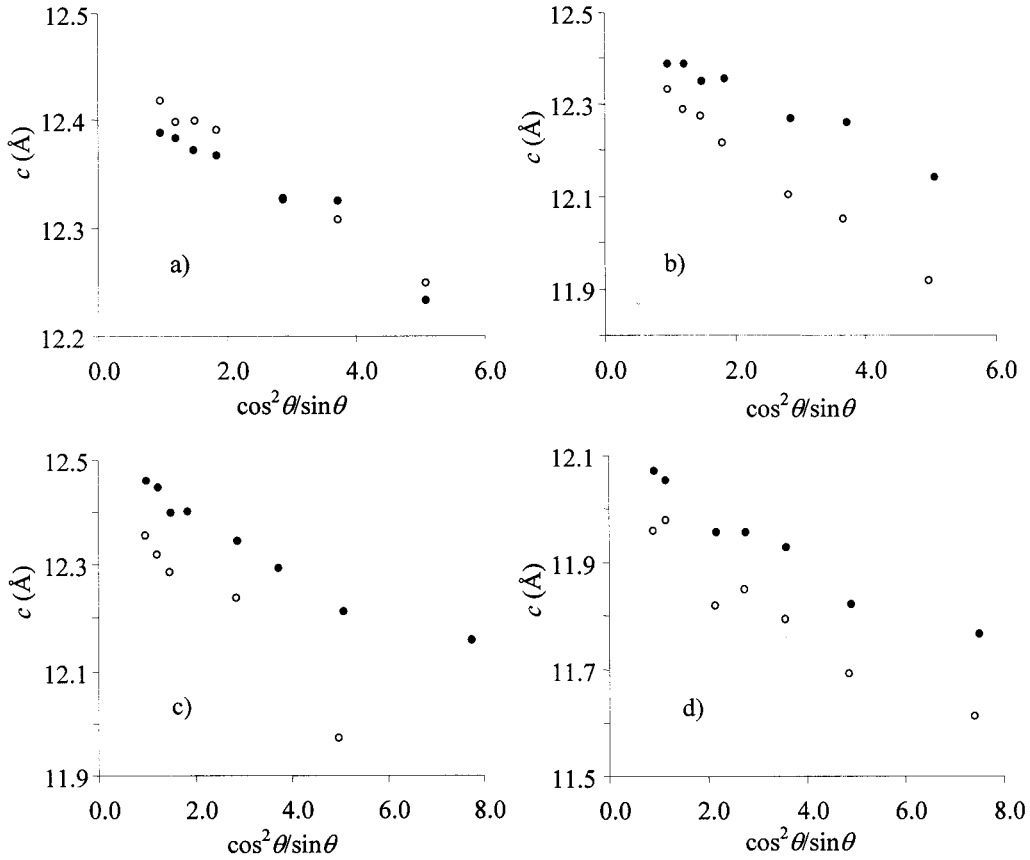

Figure 12. *c*-axis lattice parameter vs $\cos^2\theta/\sin\theta$ for (a) PBZT, (b) MePBZT, (c) DiMePBZT, and (d) MePBI: (●) sample heat-treated below the cross-linking temperature; (○) sample heat-treated at cross-linking temperatures. Data for various (00*l*) reflections used as discussed in the text.

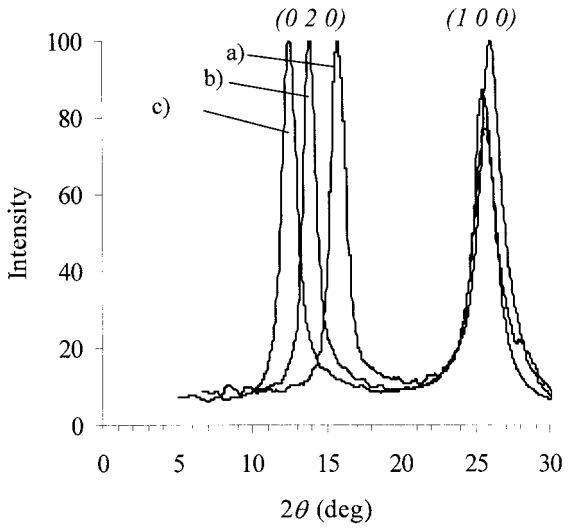

Figure 13. WAXD equatorial scans of (a) PBZT, (b) MePBZT, and (c) DiMePBZT fibers heat-treated under tension at 400 °C.

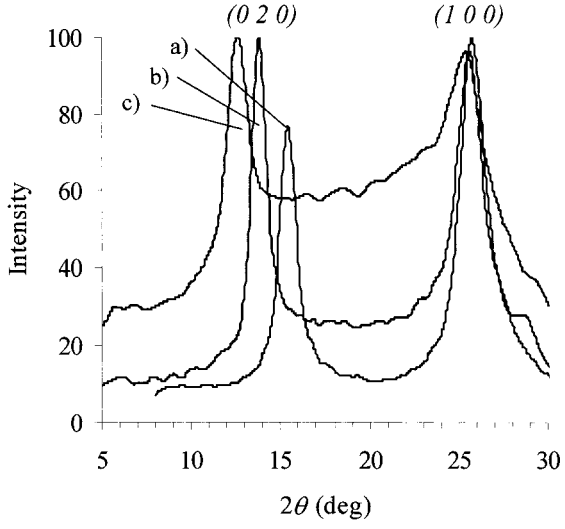

Figure 14. WAXD equatorial scans of (a) PBZT, (b) MePBZT, and (c) DiMePBZT fibers free annealed at 490 °C.

eter for PIPD is 12.01 Å.[36] When heated above the degradation temperature, the value of the *c*-axis lattice parameter of MePBI decreased to 11.98 Å, a decrease of 0.9%.

Perturbation of the crystal is also observed in equatorial scans of MePBZT and DiMePBZT before and after pendant cleaving. Equatorial WAXD scans for PBZT, MePBZT, and DiMePBZT, before and after cross-linking, are presented in Figures 13 and 14. As-spun PBZT fiber, tension heat-treated under similar conditions to that of the methyl pendant polymers, was used for purposes of comparison. Major equatorial *d* spacings are listed in Table 3. Figure 13 shows a systematic increase in the (0 2 0) interplanar spacing, attributable to the increased volume necessary to incorporate the methyl pendant groups in MePBZT and DiMePBZT. Upon heat treatment above cross-linking temperatures, changes in peak positions are noticeable in all systems. Shifting of peak positions in PBZT is a result of slight molecular reorganization due to heat treatment. It should be noted that several lower intensity peaks, observed in highly oriented PBZT fibers,[37] are not well resolved in the

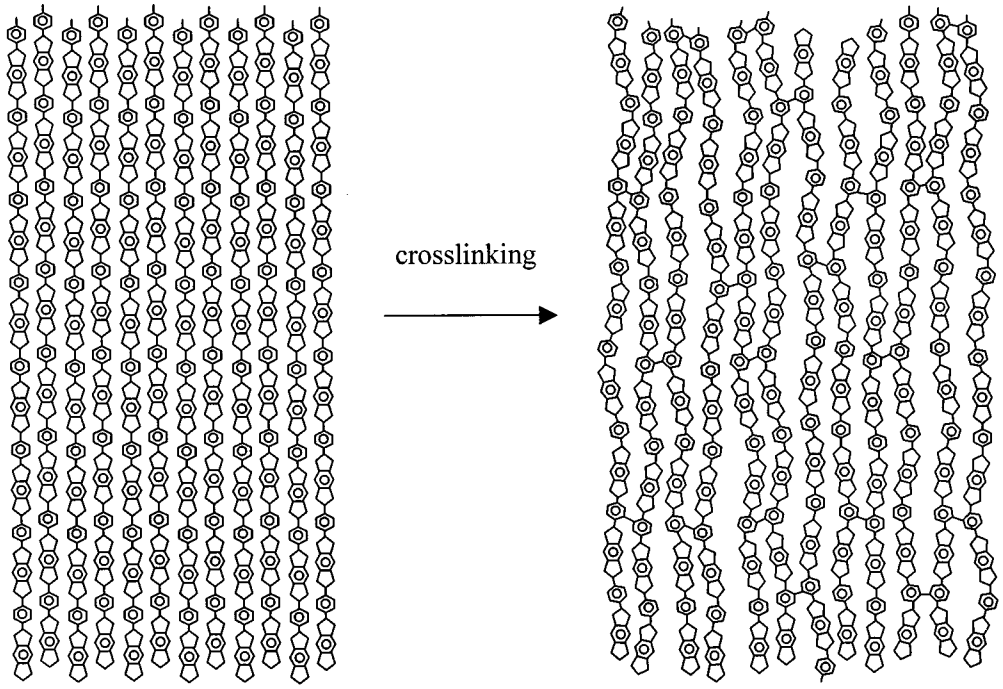

Figure 15. Schematic illustrating the perturbations in MePBZT and related rigid-rod polymers upon cross-linking.

Table 3. Major Equatorial Diffraction Peak Positions for MePBZT and DiMePBZT before and after Heat Treatment at Cross-Linking Temperatures; Data for PBZT Are Given for Comparison

system	heat treatment temp (°C)	major equatorial diffraction peaks (2θ deg)	
PBZT	400 (tension)	15.95	25.55
	490 (free)	15.50	25.80
MePBZT	400 (tension)	13.90	26.05
	490 (free)	13.80	25.65
DiMePBZT	350 (tension)	12.55	25.75
	490 (free)	12.60	25.45

equatorial scans presented in Figure 13. However, the observed peak positions in PBZT compare favorably with those previously reported for other similarly oriented PBZT fibers.[19] In MePBZT, the shift of the peak at 26.05° 2θ (3.42 Å) to approximately 25.65° 2θ (3.47 Å) suggests lateral expansion. Similar movement of the peak at 25.75° 2θ (3.46 Å) to 25.45° 2θ (3.50 Å) is also observed in DiMePBZT. In either case, the *d* spacing approaches that found in PBZT. Systematic changes in the (1 0 0) plane spacing are not observed. While some shifting of this peak takes place in both MePBZT and DiMePBZT diffraction patterns, the plane spacing increases in one while decreasing in the other. Figure 13 would suggest that this plane would be most sensitive to the disappearance of methyl groups. However, the lack of a consistent shift of this peak does not allow for an immediate interpretation. A notable difference between Figures 13 and 14 is the disproportionate increase in background between the (0 2 0) and (1 0 0) planes, in scans of MePBZT and DiMePBZT after cross-linking. This can be seen in comparing parts a and b of Figure 14, where the background intensity in the low 2θ region is comparable. It is also interesting that the ratio of peak intensity to background is much less in the case of DiMePBZT, due to substantial loss of crystallinity in DiMePBZT on free annealing leading to cross-linking.

From the reported crystalline model of PBZT,[32] the closest distance between any two atoms, other than hydrogen, is on the order of 3 Å. It has been suggested that crystalline perturbations, resulting from relatively short carbon−carbon cross-links (i.e., approximately 1.54 Å in length), would explain the accelerated axial contraction observed to occur upon pendant cleaving.[20] Resultant perturbations, as visualized in Figure 15, may also offer an explanation for the disproportionate increase in background scattering observed in Figure 14. It should not be surprising that anisotropic residual stresses and strains may result upon cross-linking in these highly anisotropic systems. In this regard, it may be advantageous to design cross-linkable systems where perturbation of the material upon cross-linking would be minimal. Moreover, since cross-linking reaction results in enhanced axial shrinkage, questions remain as to the effect of a constraining force during heat treatment on the cross-linking reaction. Some observations have already been made in this regard that suggests that stress hinders cross-linking.[19] These observations are consistent with the thermal analysis results detailed in this work; however, thus far they have not been substantiated via spectroscopic techniques.

Acknowledgment. This effort was partially sponsored by the Air Force Office of Scientific Research, Air Force Materials Command, USAF, under Grant F49620-00-1-0147.

Appendix

The following analysis was applied to determine the functional form of the systematic error for sample displacement in transmission geometry. A schematic of the effect of sample displacement on peak position is presented in Figure 16. Undisplaced sample is rotated about point O. **N** is a vector normal to the diffraction plane and bisects the angle 180° − 2θ. R_0 is the diffractometer radius, and R is the diffractometer radius relative to the displaced sample. If $R \gg D$, then $R \approx R_0$. D is the sample displacement at some sample rotation angle θ. However, as the sample is rotated, the apparent displacement, that is the displacement seen

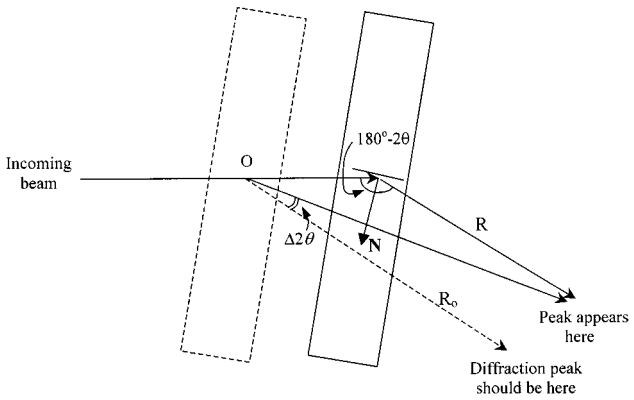

Figure 16. Schematic illustrating the effect of sample displacement on peak position, $\Delta 2\theta$.

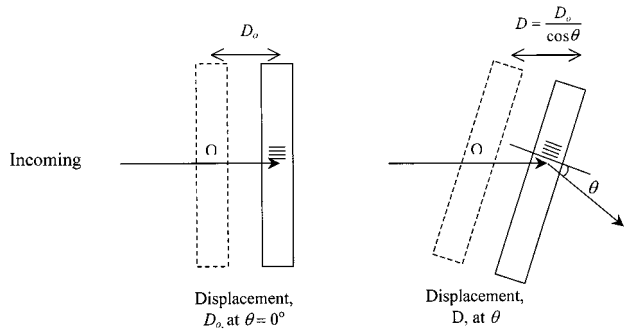

Figure 17. Effect of sample rotation in a $\theta/2\theta$ scan on apparent displacement.

by the beam, increases by a factor $(\cos\theta)^{-1}$ (Figure 17). It is also important to note that if we define δ to be the displacement parallel to the diffraction plane normal, similar to what was done in the case of reflection, then from Figure 16 we see that

$$\delta = D \sin\theta$$

Including, in this equation, the effect of sample rotation on the displacement yields

$$\delta = D_0 \frac{\sin\theta}{\cos\theta} \tag{1}$$

Returning to Figure 16, we can write the following relation

$$\frac{\sin(\Delta 2\theta)}{D_0/\cos\theta} = \frac{\sin(180 - 2\theta)}{R_0}$$

Simplifying and assuming $\Delta 2\theta$ to be small, we arrive at

$$\Delta\theta \cong \frac{D_0}{R_0} \sin\theta \tag{2}$$

Solving eq 1 for D_0 and inserting into eq 2 expresses $\Delta\theta$ in terms of δ. In particular

$$\Delta\theta \cong \frac{\delta}{R_0} \cos\theta \tag{3}$$

Inserting eq 3 into the differentiated form of Bragg's law gives the functional form of the systematic error for a sample displacement in transmission geometry. Namely,

$$\frac{\Delta d}{d} = -\frac{\delta}{R_0} \frac{\cos^2\theta}{\sin\theta}$$

which is analogous to reflection. It should be noted again that other sources of error in measured d spacing, such as absorption, have been neglected.

References and Notes

(1) (a) Kumar, S.; Helminiak, T. E. *Mater. Res. Soc. Symp. Proc.* **1989**, *134*, 363. (b) Kozey, V. V.; Jiang, H.; Mehta, V. R.; Kumar, S. *J. Mater. Res.* **1995**, *10*, 1044.
(2) Kovar, R. F.; Haghighat, R. R.; Lusignea, R. W. *Mater. Res. Soc. Symp. Proc.* **1989**, *134*, 389.
(3) Hwang, C. R.; Malone, M. F.; Farris, R. J.; Martin, D. C.; Thomas, E. L. *J. Mat. Sci.* **1991**, *26*, 2365.
(4) Lee, C. Y.-C.; Santhosh, U. *Polym. Eng. Sci.* **1993**, *33*, 907.
(5) Rein, D. M.; Cohen, Y. *J. Mater. Sci.* **1995**, *30*, 3587.
(6) Wang, C. S.; Burkett, J.; Bhattacharya, S.; Chuah, H. H.; Arnold, F. E. *Polym. Mater. Sci. Eng.* **1989**, *650*, 767.
(7) Dean, D. R.; Husband, D. M.; Dotrong, M.; Wang, C. S.; Dotrong, M. H.; Click, W. E.; Evers, R. C. *J. Polym. Sci., Polym. Chem.* **1997**, *35*, 3457.
(8) L.-S. Tan, Arnold, F. E.; Dang, T. D.; Chuah, H. H.; Wei, K. H. *Polymer* **1994**, *35*, 14.
(9) Sikkema, D. J. *Polymer* **1998**, *39*, 5981.
(10) Dang, T. D.; Wang, C. S.; Click, W. E.; Chuah, H. H.; Tsai, T. T.; Husband, D. M.; Arnold, F. E. *Polymer* **1997**, *38*, 621.
(11) Bhattacharya, S.; Chuah, H. H.; Dotrong, M.; Wei, K. H.; Wang, C.-S.; Vezie, D.; Day, A.; Adams, W. W. *Polym. Mat. Sci. Eng., ACS* **1989**, *60*, 512.
(12) Santhosh, U.; Dotrong, M. H.; Song, H. H.; Lee, C. Y.-C. *Polym. Mat. Sci. Eng., ACS*, **1991**, *65*, 40.
(13) Sweeney, W. *J. Polym. Sci.: Polym. Chem.* **1992**, *30*, 1111.
(14) Ricket, C.; Neuenschwander, P.; Suter, U. W. *Macromol. Chem. Phys.* **1994**, *195*, 511.
(15) Jiang, T.; Rigney, J.; Jones, M. G.; Markoski, L. J.; Spilman, G. E.; Mielewski, D. F.; Martin, D. C. *Macromolecules* **1995**, *28*, 3301.
(16) So, Y.-H.; Bell, B.; Heeschen, J. P.; Nyquist, R. A.; Murlick, C. L. *J. Polym. Sci., Polym. Chem.* **1995**, *33*, 159.
(17) Hu, X.; Kumar, S.; Polk, M. B.; VanderHart, D. L. *J. Polym. Sci.: Polym. Chem.* **1998**, *36*, 1407.
(18) Hu, X.; Polk, M. B.; Kumar, S. *Macromolecules*, in press.
(19) Mehta, V. R.; Kumar, S. *J. Appl. Polym. Sci.* **1999**, *73*, 305.
(20) Jenkins, S.; Jacob, K. I.; Kumar, S. *J. Polym. Sci., Polym. Phys.* **1998**, *36*, 3057.
(21) Mehta, V. R.; Kumar, S.; Polk, M. B.; VanderHart, D. L.; Arnold, F. E.; Dang, T. D. *J. Polym. Sci., Polym. Phys.* **1996**, *34*, 1881.
(22) Kuroki, T.; Tanaka, Y.; Hokudoh, T.; Yabuki, K. *J. Appl. Polym. Sci.* **1997**, *65*, 1031.
(23) Arnold, F. E., private communication.
(24) Kumar, S. *Indian Fiber, J. Text. Res.* **1991**, *16*, 52.
(25) Im, J. Percha, P. A.; Yeakle, D. S. *Mater. Res. Soc. Symp. Proc.* **1989**, *134*, 307.
(26) Reynolds, W. N. *Physical Properties of Graphite*; Elsevier Publishing Co.: New York, 1968.
(27) Jones, E. G.; Pedrick, D. L. *Mater. Res. Soc. Symp. Proc.* **1989**, *134*, 407.
(28) Jiang, H.; Desai, P.; Kumar, S.; Abhiraman, A. S. *Carbon* **1991**, *29*, 635.
(29) Lenhert, P. G.; Adams, W. W. *Mater. Res. Soc. Symp. Proc.* **1989**, *134*, 329.
(30) Cullity, B. D. *Elements of X-ray Diffraction*, 2nd ed.; Addison-Wesley Publishing: Reading, MA, 1978.
(31) Cohen, J. B. *Diffraction Methods in Material Science*; Macmillan: New York, 1966.
(32) Farmer, B. L.; Chapman, B. R.; Dudis, D. S.; Adams, W. W. *Polymer* **1993**, *34*, 1588.
(33) Macturk, K. S.; Eby, R. K.; Farmer, B. L. *Polymer* **1994**, *35*, 53.
(34) Price, G. E.; Kumar, S., unpublished results.
(35) Fratini, A. V.; Lenhert, P. G.; Resch, T. J.; Adams, W. W. *Mater. Res. Soc. Symp. Proc.* **1989**, *134*, 431.
(36) Klop, E. A.; Lammers, M. *Polymer* **1989**, *39*, 5987.
(37) Fratini, A. L.; Lenhert, P. G.; Resch, T. J.; Adams, W. W. *Mater. Res. Soc. Symp. Proc.* **1989**, *134*, 431.

MA000780W